Asymmetric phosphoinositide lipid bilayers generated by spontaneous lipid insertion

Gwendal Guerin[1], Thi Lan Anh Nguyen[1], John Manzi[1], Christophe Le Clainche[2], Julien Heuvingh[3], Nicolas Rodriguez[4], Sophie Cribier[4], Julien Berro[5], and Feng-Ching Tsai[1*]

1. Institut Curie, Université PSL, Sorbonne Université, CNRS UMR168, Laboratoire Physico-Chimie Curie, 75005 Paris, France
2. Université Paris-Saclay, CEA, CNRS, Institute for Integrative Biology of the Cell (I2BC), 91198 Gif-sur-Yvette, France
3. PMMH, ESPCI ParisPSL University, CNRS, Université Paris Cité, Sorbonne Université Paris France
4. Sorbonne Université, École Normale Supérieure, PSL University, CNRS, Laboratoire des Biomolécules, LBM, 75005, Paris, France
5. Department of Molecular Biophysics and Biochemistry, Yale University, New Haven, Connecticut, USA

*Corresponding author: feng-ching.tsai@curie.fr

Abstract

Phosphatidylinositol phosphate (PIP) lipids, located on the inner leaflet of the membrane facing the cytoplasm, are key regulators of a wide range of cellular events at the plasma membrane, in some cases by interacting with partner proteins that regulate actin assembly. Supported lipid bilayers (SLBs) have been recognized as a powerful model membrane to dissect the mechanisms underlying the clustering and interactions of PIP lipids with their partner proteins. However, despite advances in methods to generate SLBs, it remains a challenge to robustly obtain fluid SLBs in which PIP lipids are mobile and asymmetrically distributed. In this study, we report a simple and robust method to generate asymmetric-SLBs with controllable amounts of PI(4,5)P_2 and PI by dissolving them at a concentration below their critical micellar concentration (CMC) to facilitate their insertion into the upper leaflet of the SLB exposed to the bulk solution. We validated the mobility of PI(4,5)P_2 and PI lipids in the SLBs using fluorescence recovery after photobleaching (FRAP). We demonstrated the utility of PI(4,5)P_2-asymmetric SLBs by showing that they can recruit actin-membrane linker protein ezrin and myosin 1 motors, which are capable of sliding actin filaments on the SLBs. We expect our new method for preparing asymmetric-SLB to be applicable to the incorporation of other high CMC lipid species.

Introduction

The membranes of eukaryotic cells consist of a lipid bilayer containing a remarkable diversity of lipid species and proteins that serve as a physical barrier for the cells and organelles[1]. The asymmetric distribution of lipid species is a fundamental feature of cell membranes. A prominent example is the plasma membrane where sphingomyelin (SM) is abundant in the exoplasmic leaflet, whereas phosphatidylethanolamine (PE), phosphatidylserine (PS), and notably phosphatidylinositol (PI) lipids are predominantly found in the cytoplasmic leaflet[2]. PI lipids account for ~10% of total phospholipid[3]. Despite being a minor lipid species in the plasma membrane, PI and its phosphorylated derivatives, phosphatidylinositol phosphate (PIP) lipids, are recognized as key cellular regulators, affecting

numerous processes such as membrane trafficking, lipid signaling pathways and actin cytoskeleton assembly[4]. The synthesis of PIP lipids is spatiotemporally controlled, resulting in their enrichment at specific membrane regions to regulate their effector proteins. PIP lipids are generated by the phosphate modifications of PI lipids on the inositol ring at the three, four, and five hydroxyl group with seven different combinations. PIP lipids exhibit a greater negative charge at the head group than PS at neutral pH, due to the presence of two negative charges per phosphate [5]. The phosphate modification enables PIP lipids to interact specifically with phosphoinositide-binding proteins including pleckstrin homology (PH), Phox (PX), and BAR domains[6]. However, the interaction dynamics of the phosphoinositide-binding proteins with specific PI lipids, for example the strength and specificity of the binding sites, or PI-mediated cooperative protein-protein interactions remain unclear.

Among the PIP lipids, PI(4,5)P_2 is the most abundant, accounting for 0.5 up to 4 mol% of the total plasma membrane lipids, estimated to be ~ 4000 up to 34, 000 molecules per μm^2 [5,6]. By interacting with hundreds of effector proteins, PI(4,5)P_2 is known to regulate a large number of cellular events involving membranes[5,7–9]. PI(4,5)P_2 has therefore been extensively studied, particularly experimentally by using *in vitro* reconstitution assays consisting of model membranes. For example, it has been found that PI(4,5)P_2 can form clusters by interacting with positively charged divalent ions [10–13], and the interactions of PI(4,5)P_2 with effector proteins such as ezrin, radixin and moesin protein family and actin nucleation promoting factors can regulate actin assembly[7–9,14–18]. Despite these revealing findings, it remains elusive how the dynamical interactions of PIP lipids and their effector proteins lead to versatile membrane processes in cells.

Supported lipid bilayers (SLBs) and membrane vesicles are widely used model membrane platforms to study lipid-lipid and protein-lipid interactions *in vitro*[19,20]. Vesicles are the closest replica of biological membranes because the two leaflets of the membrane are in contact with solutions. SLBs, on the other hand, require a substrate on which the bilayer forms. However, the substrate support stabilizes the bilayer and the planar shape of SLBs makes them the preferred choice for certain experiments involving atomic force microscopy, total internal reflection fluorescence (TIRF) microscopy, single molecule tracking and super-resolution imaging which often require the imaging plane to be close to the substrate [21–24]. Diffusion and tracking of proteins or lipids are more straightforward to quantify on SLBs than on vesicles, where three-dimensional motion and out-of-plane membrane shape fluctuations have to be taken into account[25].

Common methods for generating SLBs include Langmuir-Blodgett deposition, the fusion of small vesicles (of the order of 100 nm in diameter), the rupture of giant vesicles (μm in diameter), and rapid solvent exchange to drive SLB formation[26–29]. Vesicle fusion and rupturing can produce symmetric SLBs (sym-SLBs), where the lipid composition is the same on both leaflets. However, a problematic issue with sym-SLBs is the inherent and often undesirable interactions between the lipids and the substrates. These lipid-substate interactions are known to reduce lipid mobility, likely due to factors such as surface roughness and electrostatic interactions[30–33]. Such interactions are particularly pronounced for negatively charged lipids like PI(4,5)P_2, which can become almost completely immobilized in the bottom lipid leaflet that contacts the glass substrate[32,34–36]. To improve the mobility of the lipids in contact with the substrate, one can replace the glass substrates with mica, or coat of the substrates with polymers to create a cushion between the substrate and the lipids[37]. On the other hand, to achieve an asymmetric lipid distribution in SLBs, the Langmuir-Blodgett deposition is a robust method, but it requires sophisticated procedures[27]. Other methods include methyl-β-cyclodextrin-assisted lipid exchange to enrich sphingomyelin in the top lipid leaflet facing to the buffer[38,39], using negatively charged surfaces to promote a higher amount of negatively charged lipids in the top leaflet[40], transferring lipids to the top leaflet by the hemifusion of vesicles on the SLBs[41], and directly using asymmetric vesicles to form SLBs[42]. While these methods enable the generation of asymmetric SLBs, they are often limited to specific lipid types for asymmetric incorporation, and they do not offer precise control over the distribution of asymmetric lipids between the two leaflets. Recently, an

elegant technique has been developed to generate asymmetric SLBs for PI(4,5)P_2 using additional vector small unilamellar vesicles (SUVs) containing PI(4,5)P_2 to dope the top leaflet of the SLBs with PI(4,5)P_2, although the underlying formation mechanism remains to be identified [36]. To date, there is a lack of robust methods to generate SLBs with asymmetric distribution of PI and PIP lipids on the top leaflet of the SLBs, facilitating quantitative studies of lipid-protein interactions.

Of note, suspended planar lipid bilayers generated in micropores are an elegant approach that avoids the use of solid substrates[43]. Since the suspended planar bilayers are often generated in a stepwise manner, one leaflet at a time, it is possible to have an asymmetric bilayer. However, to generate suspended planar bilayers, it requires more sophisticated procedures than those used to generate SLBs and the usage of oil as solvent may impact lipid dynamics [44–46].

In this study, we propose a new method for preparing asymmetric supported lipid bilayers (asym-SLBs), in which PI(4,5)P_2 and PI, are present only in the top leaflet of the SLBs. Inspired by the recently developed method using vector SUVs[36], our approach leverages lipids of interest with a high critical micellar concentration (CMC). In our method, the lipids of interest can spontaneously insert into pre-formed SLBs by dissolving the lipids in a solution at a concentration lower than their CMC. Similar procedures have been used to stain cell or model membranes using lipophilic dyes such as Dil and amphiphilic dyes such as Laurdan[47,48]. Our method is simple and robustly reproducible. It allows control over the concentration of the lipids of interest incorporated into asym-SLBs. The asym-SLBs allow us to study the dynamics of the lipids of interest free from any interaction with the substrate. We quantitatively characterized membrane asymmetry and fluidity using fluorescently labelled PI(4,5)P_2, TopFluor-PI(4,5)P_2 (TF-PI(4,5)P_2). Our method allows the amount of TopFluor-PI(4,5)P_2 incorporation to be fine-tuned. In addition to TF-PI(4,5)P_2, we showed the utility of our method to incorporate another fluorescently labelled PI, TopFluor-TMR-PI, into TF-PI(4,5)P_2-asym-SLBs. We further demonstrated the utility of asymmetrically incorporating PI(4,5)P_2 into SLBs by recruiting the PI(4,5)P_2-associated actin-membrane linker ezrin, which in turn recruits actin to PI(4,5)P_2-asym-SLBs, as well as myosin I motor, myosin 1b, which glides single actin filaments on PI(4,5)P_2-asym-SLBs. Taken together, the asym-SLBs developed in this study provide a robust experimental model system for future quantitative studies of lipid dynamics and lipid-protein interactions *in vitro*.

Results and Discussions

The generation of asymmetric SLBs with PI(4,5)P_2

PI(4,5)P_2 was reported to have a CMC on the order of a few μM in 100 mM NaCl and 30 μM in water (Fig. 1A)[49,50]. We therefore hypothesized that dissolving PI(4,5)P_2 at a relatively high concentration in solution, but below its CMC, could facilitate its insertion into the top leaflet of pre-formed SLBs. This spontaneous lipid insertion is due to the less favorable hydrophobic interaction of the fatty acid chains of PI(4,5)P_2 with the solution than with the lipid membrane. To test our hypothesis, we first prepared a SLB containing DOPC and DOPS (9:1 molar ratio) on a glass substrate using the well-established SUV fusion method[51], and then introduced into the experimental chamber a solution of TF-PI(4,5)P_2 at a concentration below its CMC. We incubated the PI(4,5)P_2 solution with the base SLB for 10 min, allowing TF-PI(4,5)P_2 to insert into the top leaflet of the base SLB (Fig. 1B). The resulting asym-SLB was rinsed with the working buffer (0.8 mM Sodium Phosphate, 15.3 mM Sodium Chloride, 0.3 mM Potassium Chloride, 0.2 mM Potassium Phosphate and 1 mM EDTA) to remove excess TF-PI(4,5)P_2 remaining in the solution. Using 5 μM of TF-PI(4,5)P_2 in solution produced asym-SLBs with relatively homogenous fluorescence demonstrating the proper incorporation of TF-PI(4,5)P_2 on the SLBs (Fig. 2A *Left*). Using nM concentrations of TF-PI(4,5)P_2, we were able to detect individual TF-PI(4,5)P_2 on the asym-SLBs (Fig. 2B).

Comparison between asymmetric and symmetric SLBs containing PI(4,5)P_2

To quantitatively characterize the resulting asym-PI(4,5)P_2-SLBs, we performed Fluorescence Recovery After Photobleaching (FRAP) experiments to measure the diffusion coefficients of TF-PI(4,5)P_2 and its immobile fractions within the asym-SLBs, and compared them with those measured in symmetric SLBs containing PI(4,5)P_2. Given the known tendency of PI(4,5)P_2 to remain immobile when in contact with a glass substrate, the measured immobile fraction of PI(4,5)P_2 serves as an indicator of its asymmetric distribution in the two leaflets of the SLB. The time series of the FRAP images showed a clear difference between the sym- and asym-SLBs (Fig. 2A, *Right*). While the asym-PI(4,5)P_2-SLB exhibited an immobile fraction of less than 5%, the sym-PI(4,5)P_2-SLB showed much less fluorescence recovery, reflecting a higher immobile fraction of 75% on average (Fig. 2C). In the sym-SLB, the higher immobile fraction of TF-PI(4,5)P_2 can be partly attributed to the fact that 50% of the TF-PI(4,5)P_2 is in direct contact with the glass substrate, resulting in its immobilization, as previously observed[32,34–36]. Additionally, during SUV rupture, electrostatic interactions may cause PI(4,5)P_2 to migrate toward the glass substrate, further contributing to its immobilization. Although the immobile fraction is reduced to 5% in TF-PI(4,5)P_2-asym-SLBs, we did not observe 100% mobility of the lipids. This may reflect the presence of unfused SUVs in the pre-formed sym-SLBs, as previously shown by scanning electron microscopy[52]. The diffusion coefficients of TF-PI(4,5)P_2 in asym-SLBs were around 2.5 μm^2/sec, comparable to previously reported values for SLBs (Fig. 2D, asym. condition) [34,36]. As expected, we found similar diffusion coefficients for TF-PI(4,5)P_2 in both asym- and sym-SLBs (Fig. 2D). This similarity is due to the fact that the mobile lipids are only in the top leaflet in both asym- and sym-SLBs. Overall, we showed here that the proposed method based on the spontaneous insertion of PI(4,5)P_2 into pre-formed sym-SLBs allows us to generate asym-SLBs with preserved PI(4,5)P_2 fluidity.

In SLBs, lipids can flip from one leaflet to another[53]. Lipid flip-flop can lead to the loss of the asymmetric distribution of PI(4,5)P_2 over time in asym-PI(4,5)P_2-SLBs[36]. Furthermore, it has been reported that the amount of PI(4,5)P_2 in giant unilamellar vesicles (GUVs) decreases (within a few hours), due to the solubilization of PI(4,5)P_2 from the membrane into the bulk solution[54,55]. To assess to which extent PI(4,5)P_2 molecules flip-flop in the asym-PI(4,5)P_2-SLBs, we measured the lipid immobile fraction of a freshly prepared asym-SLB and compared it with the immobile fraction of asym-PI(4,5)P_2-SLBs stored a few hours after formation. We observed immobile fractions with mean values of 3% and 9% for asym-SLBs immediately after preparation and 4 hours after preparation, respectively (Fig. 2C). Our results indicate that in asym-SLBs, TF-PI(4,5)P_2 exhibits minimal flip-flop activity during the duration of our experiments, likely due to its relatively low lipophilicity.

Control of the PI(4,5)P_2 amount incorporated into the top leaflet of pre-formed SLBs

To quantify the amount of PI(4,5)P_2 incorporated into the top leaflet of the SLBs, we measured the fluorescent intensity of TF-PI(4,5)P_2 in asym-SLBs. We calibrated our measurements using TF-PI(4,5)P_2 fluorescence measurements on sym-SLBs since the concentrations of TF-PI(4,5)P_2 incorporated into the SUVs used to generate the sym-SLBs is known (Fig. S2). We found that the amount of TF-PI(4,5)P_2 incorporated into the top leaflet of asym-SLBs was directly proportional to the bulk concentration of TF-PI(4,5)P_2, up to 10 μM of TF-PI(4,5)P_2 (Fig. 3A). The use of TF-PI(4,5)P_2 at bulk concentrations ranging from 0 to 10 μM resulted in 0 to 5 mole% TF-PI(4,5)P_2 in asym-SLBs (Fig. 3A). We observed that beyond 10 μM of TF-PI(4,5)P_2, the intensity of TF-PI(4,5)P_2 did not increase significantly. This observation suggests that either the asym-SLBs were saturated with TF-PI(4,5)P_2, or the concentration of TF-PI(4,5)P_2 was high enough for the TF dyes to quench each other[11,56].

Effect of Ca^{2+} on the diffusion of PI(4,5)P_2 in asym-SLBs

Divalent ions such as calcium and magnesium are known to cluster PI(4,5)P_2 via electrostatic interactions, which can affect the immobile fraction and potentially alter the diffusion of PI(4,5)P_2[11–

[13,57,58]. To evaluate how well PI(4,5)P_2 in our PI(4,5)P_2-asym-SLBs retains its expected properties, such as its ability to diffusion or form clusters in the presence Ca^{2+} ions, we quantified the effect of Ca^{2+} on the diffusion and immobile fractions of TF-PI(4,5)P_2. By performing FRAP experiments, we observed an increase in the immobile fraction of TF-PI(4,5)P_2 in the presence of 1μM of Ca^{2+} ions compared to that without Ca^{2+} ions. The increased immobile fraction indicates PI(4,5)P_2 molecules were clustered by Ca^{2+} ions (Fig. 4A). On the other hand, the diffusion coefficient of mobile TF-PI(4,5)P_2 was only slightly affected by the presence of Ca^{2+} ions (Fig. 4B), consistent with previous reported using FCS. This observation is consistent with a previous report of a slight decrease in the diffusion of TF-PI(4,5)P_2 monomers and TF-PI(4,5)P_2 clustering in GUVs due to the presence of Ca^{2+} ions measured by fluorescence correlation spectroscopy (FCS) [10]. Our results indicated that in the presence of Ca^{2+}, the freely diffusing TF-PI(4,5)P_2 was not significantly affected by the presence of TF-PI(4,5)P_2 clusters and possibly the kinetics of clustering and de-clustering is much slower than the timescale used for measuring the FRAP recoveries.

Dual asymmetric incorporation of TF-TMR-PI and TF-PI(4,5)P_2

So far, we have demonstrated our approach to generate asym-SLBs using TF-PI(4,5)P_2 because of its relatively high CMC, which facilitates its incorporation into pre-formed SLBs. We then investigated the possibility of using our approach to generate asym-SLBs with other lipids from the phosphatidylinositol family, the fluorescently labelled PI lipid TopFluor-TMR-PI (TF-TMR-PI). To test the possibility of incorporating more than one lipid species asymmetrically, we used a 5μM solution of TF-TMR-PI and incubated it with pre-formed TF-PI(4,5)P_2-asym-SLBs. As shown in Figure 5A, we observed the incorporation of TF-TMR-PI into the TF-PI(4,5)P_2-asym-SLBs. We confirmed the fluidity of TF-TMR-PI in the asym-SLBs by performing FRAP experiments and found a diffusion coefficient of TF-TMR-PI of about 1.5μm²/s (Fig. 5B). To investigate whether the Ca^{2+} ion-driven immobilization of TF-PI(4,5)P_2 can also immobilize TF-TMR-PI, we performed FRAP experiments on TF-TMR-PI in the presence of TF-PI(4,5)P_2, with and without Ca^{2+} ions. We observed comparable diffusion coefficients of TF-TMR-PI in the presence and absence of Ca^{2+} ions (Fig. 5B). This observation indicates that the diffusion of the freely diffusing TF-TMR-PI was not affected by the presence of TF-PI(4,5)P_2 clusters. Notably, the immobile fraction of TF-TMR-PI was increased in the presence of Ca^{2+} ions (Fig. 5C). Since PI does not co-cluster with PI(4,5)P_2[11], the increased immobile fraction of TF-TMR-PI in PI(4,5)P2-asymmetric SLBs suggests that Ca^{2+} ions may be able to cluster TF-TMR-PI as they do for TF-PI(4,5)P_2.

The activity of PI(4,5)P_2-associated ezrin and molecular motor myosin 1b on PI(4,5)P_2-asym-SLBs

To further validate the use of PI(4,5)P_2-asym-SLBs, we examined the recruitment of the actin-membrane linker protein ezrin and its ability to anchor actin filaments. We incubated PI(4,5)P_2-asym-SLBs with 10 μM of AX488 labelled ezrinTD, followed by 1 μM AX647-phalloidin-labelled actin filaments. In the absence of PI(4,5)P_2, neither ezrin nor actin bound to the SLBs (Fig. 6A). However, when PI(4,5)P_2 was present, both ezrin and actin filaments were clearly recruited to the membrane (Fig. 6, A and B). Additionally, we investigate the activity of myosin I motor, myo1b, which contains on its C-terminal tail a pleckstrin homology (PH) domain capable of binding PI(4,5)P_2[59]. We incubated PI(4,5)P_2-asym-SLBs with 1 μM myo1b and 50 nM of AX647-phalloidin labelled actin filaments to perform motility assays[60]. As expected, we observed the gliding of the actin filaments on asym-SLB containing TF-PI(4,5)P_2 or non-fluorescently labelled PI(4,5)P_2 (Fig. 7A). The resulting actin gliding velocities are 57 nm/sec for TF-PI(4,5)P_2 and 62 nm/sec for non-fluorescently labelled PI(4,5)P_2, both comparable to those previously measured for myo1b on PI(4,5)P_2-sym-SLBs (Fig. 7B and 6C)[61].

Conclusion

In this study, we introduced a simple two-step method to generate supported bilayers with leaflets that possess distinct lipid compositions. We demonstrated the feasibility of the method by enriching one leaflet with PI(4,5)P_2, fluorescent TF-PI(4,5)P_2, and fluorescent TMR-PI. We quantitatively characterized the fluidity of the SLBs. In addition, we showcased the utility of PI(4,5)P_2-asymmetric SLBs by recruiting ezrin and myo1 motors. Our study suggests the potential application of this method to incorporate other lipids with sufficiently high CMC values, such as the other members of the phosphoinositide family and fluorescently labelled lipids[62]. While our study focused on the incorporation of lipids into SLBs, the possibility of adapting the method to other model membranes such as giant unilamellar vesicles (GUVs), large unilamellar vesicles (LUVs), and suspended planar lipid bilayers, or to the plasma membrane of cells[63], could open up the potential applications in the study of asymmetric membranes.

Figures

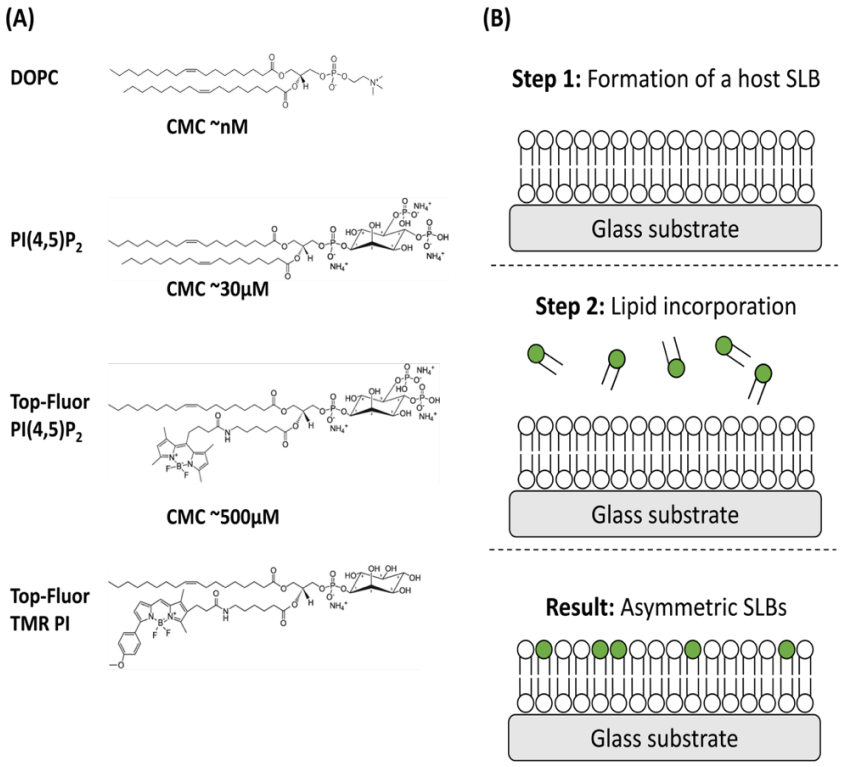

Figure 1. Schematics of the proposed mechanism for asym-SLB formation. (A) Molecular structures of the lipids used in this study, along with their approximate CMC when available[49]. (B) Step 1: Introducing a solution containing lipids of interest onto a pre-formed SLB. Step 2: allowing the lipids to incorporate into the SLB to form an asymmetric-SLB.

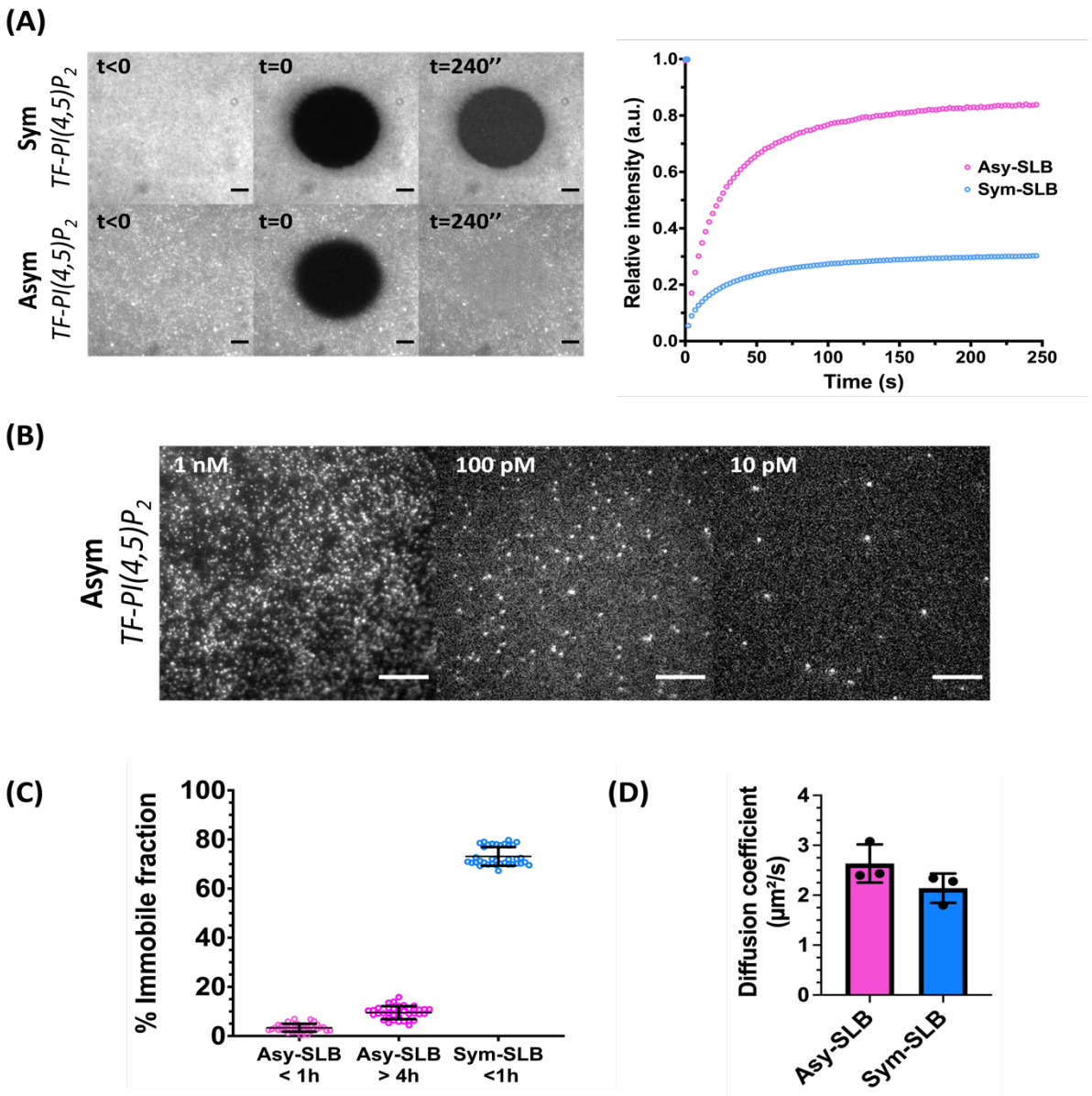

Figure 2. Quantitative comparison of sym- and asym-SLBs for TF-PI(4,5)P_2 (A) *Left panel*. Representative confocal images of FRAP experiments on TF-PI(4,5)P_2 in sym- and asym-SLBs before bleaching (t<0), immediately after bleaching (t=0) and after recovery (t=240 sec). Scale bars, 5μm. *Right*. Representative relative fluorescent intensities of the bleached area overtime, showing ~80% and ~30% recovery of TF-PI(4,5)P_2 in an asym-SLB (Magenta circles) and a sym-SLB (Cyan circles), respectively. (B) Representative image of single TF-PI(4,5)P_2 singles on asym-SLBs at various TF-PI(4,5)P_2 bulk concentration. Scale bars, 2 μm. (C) Quantification of the immobile fractions of TF-PI(4,5)P_2 in FRAP experiments performed within one hour (<1h) and four hours (>4h) after asym- and sym-SLB formation. n = 36 FRAP measurements, N = 3 independent experiments. The immobile fractions were calculated by data fitting to the FRAP curves. (D) Diffusion coefficients of TF-PI(4,5)P_2 in asym- and sym-SLB. For the asym-SLBs, TF-PI(4,5)P_2 bulk concentration was 5 μM. n = 36 FRAP measurements, N = 3 independent experiments for both asym- and sym-SLBs. Within each experiment, there were 4 different bleaching area sizes and 3 FRAP measurements were performed for each size. Data points represent the diffusion coefficients for each experiment, obtained from the linear fit of bleached areas to their recovery characteristic time (as shown in Fig. S1). The error bar represents the standard deviation of the 3 FRAP experiments.

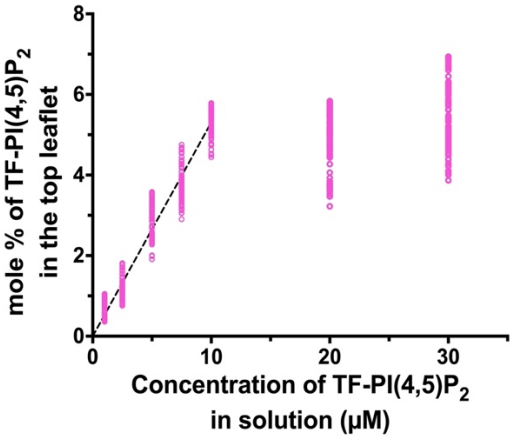

Figure 3. Control of TF-PI(4,5)P_2 incorporation into asym-SLBs. Quantification of the molar percentages of TF-PI(4,5)P_2 in the top leaflet of asym-SLB generated by using different bulk concentrations of TF-PI(4,5)P_2. The dashed black line is a linear regression of all the data points < 10µM, slope = 0.53, n = 568 measurements, N = 7 independent experiments.

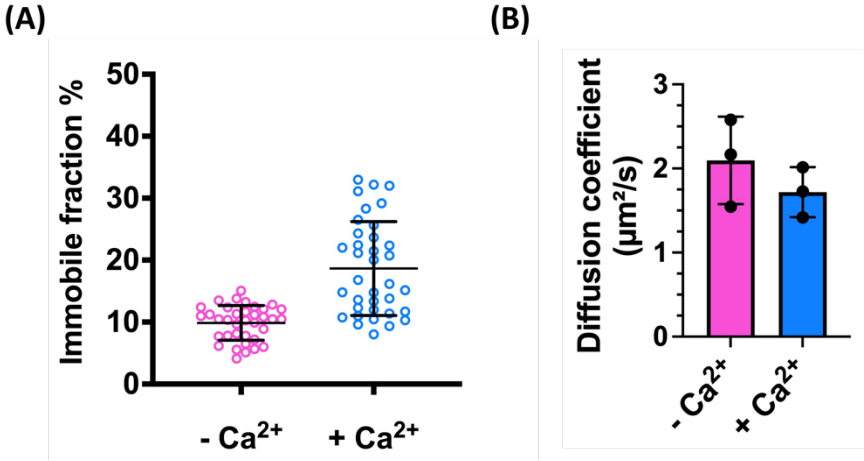

Figure 4. Effect of Ca^{2+} ions on TF-PI(4,5)P_2 diffusion and immobile fraction. (A) Measured immobile fraction of TF-PI(4,5)P_2, asymmetrically incorporated using a 5 µM TF-PI(4,5)P2 solution and in the presence or absence of 1mM of Ca^{2+} ions. In the condition "- Ca $^{2+}$", the working buffer is supplemented with 1µM of EDTA to sequester Ca^{2+} ions. In the condition "+ Ca $^{2+}$", we included 1 mM of $CaCl_2$ in the working buffer without EDTA. **(B)** Diffusion coefficients of TF-PI(4,5)P_2 in the presence and absence of Ca^2 ions. For both (A) and (B), n = 36 FRAP measurements, N = 3 independent experiments. Within each experiment, there were 4 different bleaching area sizes and 3 FRAP measurements were performed for each size. Data points represent the diffusion coefficients for each experiment. The error bar represents the standard deviation of the 3 FRAP experiments.

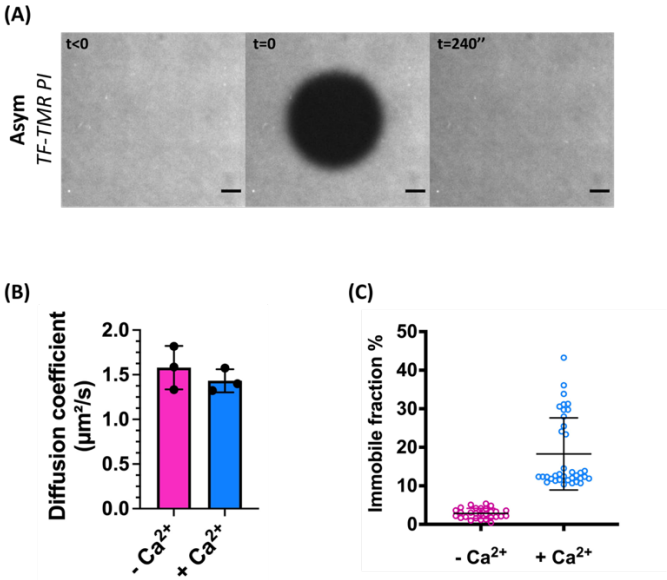

Figure 5. Asymmetric incorporation of TF-TMR-PI into asym-PI(4,5)P_2 SLBs. (A) Confocal images of FRAP experiments on TF-TMR-PI asymmetrically incorporated into TF-PI(4,5)P_2-asym-SLBs by using a 5µM of TF-TMR-PI solution, before bleaching (t<0), immediately after bleaching (t=0) and after recovery (t=240"). Scale bars, 5µm. **(B)** Diffusion coefficients of TF-TMR-PI in the presence and absence of 1mM Ca^{2+} ions. For both conditions, n = 36 FRAP measurements, N = 3 independent experiments. Within each experiment, there were 4 different bleaching area sizes and 3 FRAP measurements were performed for each size. Data points represent the diffusion coefficients for each experiment. The error bar represents the standard deviation of the 3 FRAP experiments. **(C)** Immobile fraction of TF-TMR-PI in the presence and absence of 1mM Ca^{2+}ions. For all experiments, the TF-PI(4,5)P_2-asym-SLBs were formed using a 5µM TF-PI(4,5)P_2 solution. For both conditions, n = 36 FRAP measurements, N = 3 independent experiments.

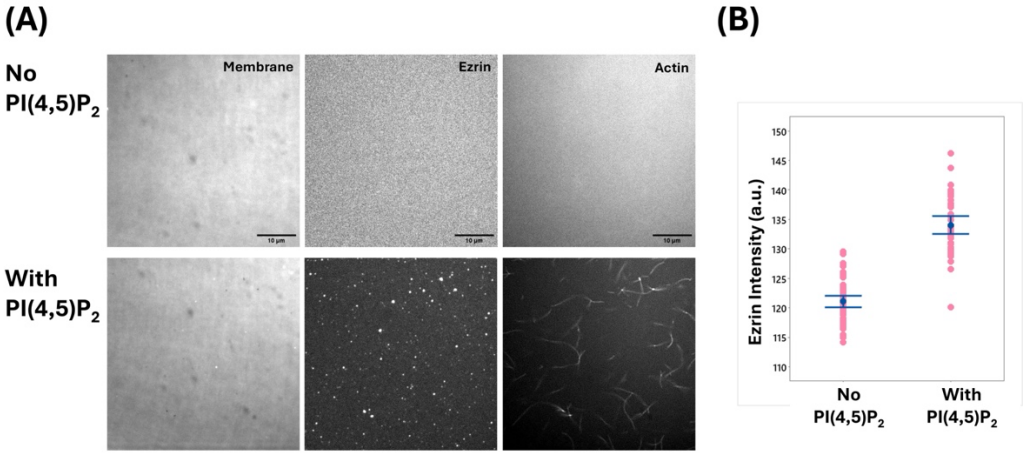

Figure 6. Actin filament recruitment by ezrinTD on PI(4,5)P_2-asym-SLBs. **(A)** Representative confocal images of xx, AX488 labelled ezrinTD and AX647 phalloidin-labelled actin filament on SLBs without PI(4,5)P_2 (*Top*) and PI(4,5)P2-containing asymmetric SLBs (*Bottom*) of PI(4,5)P_2. Scale bars, 10 µm. **(B)** Quantification of ezrin intensity on SLBs without PI(4,5)P_2 and PI(4,5)P_2-containing asymmetric SLBs. N = 3 independent experiments. Analyzed images: 60 for SLBs without PI(4,5)P_2 and 44 for PI(4,5)P_2-asymmetric SLBs.

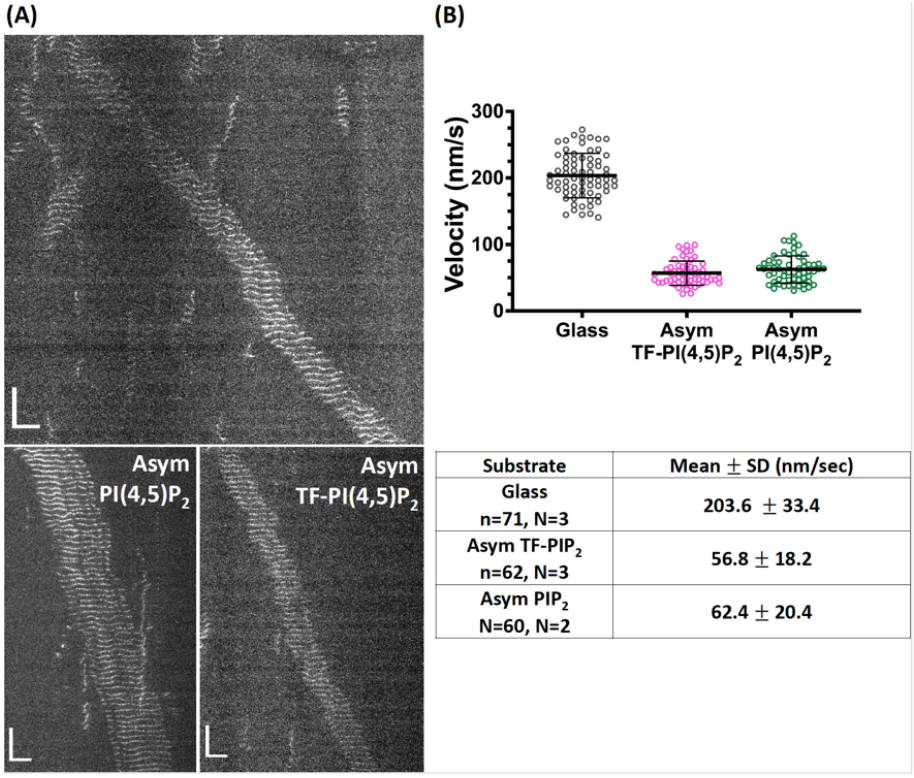

Substrate	Mean ± SD (nm/sec)
Glass n=71, N=3	203.6 ± 33.4
Asym TF-PIP$_2$ n=62, N=3	56.8 ± 18.2
Asym PIP$_2$ N=60, N=2	62.4 ± 20.4

Figure 7. Actin filament gliding by myoIb on PI(4,5)P_2-asym-SLBs. **(A)** Representative kymographs of actin filament gliding by myo1b bound on glass substrates and on asym-SLBs with PI(4,5)P_2 or TF-PI(4,5)P_2. Horizontal scale bars, 5 µm, Vertical scale bars, 1 min. Fluorescent singles were AX647 phalloidin labelled actin filaments. **(B)** Velocities of single actin filament gliding by myo1b bound on glass substrates and on asym-SLBs with PI(4,5)P_2 or TF-PI(4,5)P_2. **(C)** Table summarizes the averaged velocities of myo1b-driven actin filament gliding. n: numbers of velocity measures. N: number of independent experiments. SD: standard deviation.

Materials and Methods

Reagents

1,2-Dioleoyl-sn-glycero-3-Phosphatidylcholine (DOPC, CAS : 4235-95-4), 1,2-dioleoyl-sn-glycero-3-phospho-L-serine (DOPS, CAS: 90693-88-2), 1-oleoyl-2-[6-[4-(dipyrrometheneboron difluoride)butanoyl]amino]-hexanoyl-sn-glycero-3-phosphoinositol-4,5-bisphosphate (TF-PI(4,5)P_2, CAS: 1246355-57-6) and 1-oleoyl-2-(6-((4,4-difluoro-1,3-dimethyl-5-(4-methoxyphenyl)-4-bora-3a,4a-diaza-s-indacene-2propionyl)amino)hexanoyl)-sn-glycero-3-phosphoinositol (TF-TMR-PI, CAS: 2260795-35-3) were purchased from Avanti Polar Lipids. ATTO647N-1,2-Dioleolyl-sn-glycero-3-phosphoethanolamine (ATTO647N-DOPE, Product code: AD 647N-16) was purchased from ATTO-TEC GmbH. Other reagents were purchased from Sigma-Aldrich.

Buffer

The buffer used to dissolve the lipids and wash the SLBs, called the Working buffer, contains 0.8 mM Sodium Phosphate, 15.3 mM Sodium Chloride, 0.3 mM Potassium Chloride, 0.2 mM Potassium Phosphate and 1 mM EDTA. For PI(4,5)P_2 clustering experiments, the 1mM EDTA is replaced by 1mM $CaCl_2$. MilliQ (MQ) water was used in all buffer preparations.

Preparation of SUVs

The desired amount of lipids were mixed in $CHCl_3$ and then dried with N_2, followed by drying in a vacuum chamber for a few hours or overnight to ensure that the $CHCl_3$ was completely evaporated. The dried lipid film was hydrated with MQ H_2O at a lipid concentration of 1.5 mg/mL and incubated at room temperature for 30 min to form vesicles. The resulting vesicle suspension was vortexed, followed by sonication in a bath sonicator (Fisher Scientific, ref. 10611983, at maximum power) twice for 30 min each at room temperature to generate SUVs. The resulting SUVs were then centrifuged at 20000g for 1 hour at 4°C to remove any lipid debris. The SUV supernatant was collected and stored at 4°C for a maximum of two weeks.

Preparation of lipid solutions

The desired lipids were mixed in $CHCl_3$ and then dried with N_2, followed by drying in a vacuum chamber for a few hours or overnight to ensure that the $CHCl_3$ was completely evaporated. The resulting lipid film was resuspended in the working buffer to obtain a final lipid concentration of 10µM for PI(4,5)P_2, TF-PI(4,5)P_2, and TF-TMR-PI. The lipid solution was either stored at 4°C for a maximum of two weeks or at -20°C for several months.

Preparation of Sym-SLBs

Glass coverslips were first cleaned by sonication in the following solutions for 20 min each: H_2O, Acetone, H_2O, 1M KOH and 5 times with H_2O. The coverslips were dried with N_2 and stored under vacuum before use. The experimental chamber was assembled from two cleaned coverslips glued together using double sided tapes, with the bottom coverslip plasma cleaned for 3 min to make it hydrophilic. The chamber was filled with SUVs at 0.5 mg/mL, supplemented with 1mM $CaCl_2$, followed by incubation at room temperature for 30 min to form SLBs. The resulting SLB was rinsed with 200µL working buffer (~10 times the chamber volume). The SLB was used immediately for experiments.

Preparation of Asym-SLBs

After the formation of the Sym-SLBs, the chamber was filled with a lipid solution of the lipids of interest for 10 min, followed by rinsing with 100 µL working buffer. The asym-SLB was used immediately for experiments.

FRAP experiments and data analysis

Confocal imaging was performed on an inverted microscope (Eclipse Ti-E, Nikon) equipped with a spinning disk CSU-X1 (Yokogawa), a sCmos camera Prime 95B (Photometrics) and a 60X objective (NA 1.40, oil, Nikon). A laser bench of four lines (405nm, 491nm, 561nm, 642nm; Gataca Systems) was used for FRAP and acquisition at 491 nm and 561 nm. The fluorescent intensities at each time points were obtained using Metamorph software (Gataca Systems). For each image, the intensity of the bleached area was corrected with the intensity of an unbleached area, far from the bleached region, to account for photobleaching and potential variation of the intensity overtime. For each experimental condition, we performed FRAP with four bleaching areas with diameters of 9.2 µm, 16.5 µm, 23.8 µm and 31.2 µm. We performed three FRAP experiments for each area sizes. The analysis of the FRAP curves and the extraction of characteristic time and immobile fraction were performed by using Wolfram[64]. The diffusion coefficient was obtained by fitting the diffusion coefficient using the following equation: $D = \frac{d^2}{16\tau}$ and the values of d and τ obtained for each individual sample, D is the diffusion coefficient, d is the diameter of the bleached area, and τ is the characteristic time of the FRAP recovery curve. (See supplementary figure 2)

Protein purification

Human myosin 1b was purified from HEK293-Flp-In cells following the method described previously[65]. Myo1b was stored in the following buffer: 30mM Hepes pH 7.5, 150mM KCl, 4mM $MgCl_2$, 1mM EGTA, 0.1% Methylcellulose, 4mM Na_2ATP, 1mM DTT. Muscle actin was purified from rabbit muscle and isolated in monomeric form in actin buffer (5 mM Tris-HCl, pH 7.8, 0.1 mM CaCl2, 0.2 mM ATP, 1 mM DTT and 0.01% NaN3)[66].

Preparation and analysis of motility assays

The actin motility assays were performed and analyzed following the method described previously[61]. Briefly, myo1b at 600 nM was incubated in the experimental chambers with glass substrates or $PI(4,5)P_2$-asym-SLBs for 30 min at room temperature. A 50 nM solution of pre-polymerized actin filaments (in 5 mM Tris-HCl, pH 7.8, 3 mM $MgCl_2$, 2 mM ATP, 10 mM DTT, 1mM DABCO, 100mM KCl, 0.3% Methylcellulose, 0.2mM EGTA) stabilized with AX647 phalloidin was introduced into the experimental chambers. The samples were observed using TIRF microscopy (Eclipse Ti inverted microscope, 100X TIRF objective, Quantem512SC camera). The experiments were controlled using the software Metamorph.

Acknowledgment

We thank Frederic Pincet for helping on the FRAP analysis and careful reading of the manuscript. F.-C.T. is a member of the CNRS consortium Approches Quantitatives du Vivant (AQV), Labex Cell(n)Scale (ANR-11-889 LABX0038) and Paris Sciences et Lettres (ANR-10-IDEX-0001-02). G.G., T. L. A. Nand F.-C.T. are funded by ANR grant ANR-20-CE11-0010-01 (ActinFission). G.G. and F.-C.T., J.H., S.C., N.R.,and J.B. are funded by a PSL-Qlife grant (MyoMemActin). The authors greatly acknowledge the Cell and Tissue Imaging (PICT-IBiSA), Institut Curie, member of the French National Research Infractucture France-BioImaging (ANR10-INBS-04). We thank Patricia Bassereau and Julien Pernier for fruitful discussions.

Reference

(1) Harayama, T.; Riezman, H. Understanding the Diversity of Membrane Lipid Composition. *Nat. Rev. Mol. Cell Biol.* **2018**, *19* (5), 281–296. https://doi.org/10.1038/nrm.2017.138.

(2) Lorent, J. H.; Levental, K. R.; Ganesan, L.; Rivera-Longsworth, G.; Sezgin, E.; Doktorova, M.; Lyman, E.; Levental, I. Plasma Membranes Are Asymmetric in Lipid Unsaturation, Packing and Protein Shape. *Nat. Chem. Biol.* **2020**, *16* (6), 644–652. https://doi.org/10.1038/s41589-020-0529-6.

(3) Vance, J. E. Phospholipid Synthesis and Transport in Mammalian Cells. *Traffic* **2015**, *16* (1), 1–18. https://doi.org/10.1111/tra.12230.

(4) Posor, Y.; Jang, W.; Haucke, V. Phosphoinositides as Membrane Organizers. *Nat. Rev. Mol. Cell Biol.* **2022**, *23* (12), 797–816. https://doi.org/10.1038/s41580-022-00490-x.

(5) Wills, R. C.; Hammond, G. R. V. PI(4,5)P2: Signaling the Plasma Membrane. **2022**, *0*, 2311–2325.

(6) Lemmon, M. A. Membrane Recognition by Phospholipid-Binding Domains. *Nat. Rev. Mol. Cell Biol.* **2008**, *9* (2), 99–111. https://doi.org/10.1038/nrm2328.

(7) Suetsugu, S.; Kurisu, S.; Takenawa, T. Dynamic Shaping of Cellular Membranes by Phospholipids and Membrane-Deforming Proteins. *Physiol. Rev.* **2014**, *94* (4), 1219–1248. https://doi.org/10.1152/physrev.00040.2013.

(8) Senju, Y.; Lappalainen, P. Regulation of Actin Dynamics by PI (4, 5) P2 in Cell Migration and Endocytosis. *Curr. Opin. Cell Biol.* **2019**, *56*, 7–13.

(9) Janmey, P. A.; Bucki, R.; Radhakrishnan, R. Regulation of Actin Assembly by PI (4, 5) P2 and Other Inositol Phospholipids: An Update on Possible Mechanisms. *Biochem. Biophys. Res. Commun.* **2018**, *506* (2), 307–314.

(10) Sarmento, M. J.; Coutinho, A.; Fedorov, A.; Prieto, M.; Fernandes, F. Ca2 + Induces PI(4,5)P2 Clusters on Lipid Bilayers at Physiological PI(4,5)P2 and Ca2 + Concentrations. *Biochim. Biophys. Acta - Biomembr.* **2014**, *1838* (3), 822–830. https://doi.org/10.1016/j.bbamem.2013.11.020.

(11) Wen, Y.; Vogt, V. M.; Feigenson, G. W. Multivalent Cation-Bridged PI(4,5)P2 Clusters Form at Very Low Concentrations. *Biophys. J.* **2018**, *114* (11), 2630–2639. https://doi.org/10.1016/j.bpj.2018.04.048.

(12) Wang, Y. H.; Collins, A.; Guo, L.; Smith-Dupont, K. B.; Gai, F.; Svitkina, T.; Janmey, P. A. Divalent Cation-Induced Cluster Formation by Polyphosphoinositides in Model Membranes. *J. Am. Chem. Soc.* **2012**, *134* (7), 3387–3395. https://doi.org/10.1021/ja208640t.

(13) Yu-Hsiu Wang, D. R. S. and P. A. J. Counterion-Mediated Cluster Formation by Polyphosphoinositides. *Chem Phys Lipids* **2014**, *182* (1), 38–51. https://doi.org/10.1016/j.chemphyslip.2014.01.001.Counterion-mediated.

(14) Bezanilla, M.; Gladfelter, A. S.; Kovar, D. R.; Lee, W.-L. Cytoskeletal Dynamics: A View from the Membrane. *J. Cell Biol.* **2015**, *209* (3), 329–337. https://doi.org/10.1083/jcb.201502062.

(15) Tsai, F.-C.; Guérin, G.; Pernier, J.; Bassereau, P. Actin-Membrane Linkers: Insights from Synthetic Reconstituted Systems. *Eur. J. Cell Biol.* **2024**, *103* (2), 151402. https://doi.org/10.1016/j.ejcb.2024.151402.

(16) Liebe, N. L.; Mey, I.; Vuong, L.; Shikho, F.; Geil, B.; Janshoff, A.; Steinem, C. Bioinspired Membrane Interfaces: Controlling Actomyosin Architecture and Contractility. *ACS Appl. Mater. Interfaces* **2023**, *15* (9), 11586–11598. https://doi.org/10.1021/acsami.3c00061.

(17) McClatchey, A. I. ERM Proteins at a Glance. *J. Cell Sci.* **2014**, *127* (15), 3199–3204. https://doi.org/10.1242/jcs.098343.

(18) Maniti, O.; Carvalho, K.; Picart, C. Model Membranes to Shed Light on the Biochemical and Physical Properties of Ezrin/Radixin/Moesin. *Biochimie* **2013**, *95* (1), 3–11. https://doi.org/10.1016/j.biochi.2012.09.033.

(19) Dimova, R.; Marques, C. *The Giant Vesicle Book*; CRC Press, 2019.

(20) Chan, Y.-H. M.; Boxer, S. G. Model Membrane Systems and Their Applications. *Curr. Opin. Chem. Biol.* **2007**, *11* (6), 581–587. https://doi.org/10.1016/j.cbpa.2007.09.020.

(21) Morandat, S.; Azouzi, S.; Beauvais, E.; Mastouri, A.; El Kirat, K. Atomic Force Microscopy of Model Lipid Membranes. *Anal. Bioanal. Chem.* **2013**, *405* (5), 1445–1461. https://doi.org/10.1007/s00216-012-6383-y.

(22) Oreopoulos, J.; Yip, C. M. Probing Membrane Order and Topography in Supported Lipid Bilayers by Combined Polarized Total Internal Reflection Fluorescence-Atomic Force Microscopy. *Biophys. J.* **2009**, *96* (5), 1970–1984. https://doi.org/10.1016/j.bpj.2008.11.041.

(23) Matysik, A.; Kraut, R. S. Preparation of Mica Supported Lipid Bilayers for High Resolution Optical Microscopy Imaging. *J. Vis. Exp. JoVE* **2014**, No. 88, 52054. https://doi.org/10.3791/52054.

(24) Niederauer, C.; Nguyen, C.; Wang-Henderson, M.; Stein, J.; Strauss, S.; Cumberworth, A.; Stehr, F.; Jungmann, R.; Schwille, P.; Ganzinger, K. A. Dual-Color DNA-PAINT Single-Particle Tracking Enables Extended Studies of Membrane Protein Interactions. *Nat. Commun.* **2023**, *14* (1), 4345. https://doi.org/10.1038/s41467-023-40065-8.

(25) Ohta, T. Brownian Motion on a Fluctuating Random Geometry. *J. Phys. Soc. Jpn.* **2020**, *89* (7), 074001. https://doi.org/10.7566/JPSJ.89.074001.

(26) Ferhan, A. R.; Yoon, B. K.; Park, S.; Sut, T. N.; Chin, H.; Park, J. H.; Jackman, J. A.; Cho, N.-J. Solvent-Assisted Preparation of Supported Lipid Bilayers. *Nat. Protoc.* **2019**, *14* (7), 2091–2118. https://doi.org/10.1038/s41596-019-0174-2.

(27) Kurniawan, J.; Ventrici de Souza, J. F.; Dang, A. T.; Liu, G.; Kuhl, T. L. Preparation and Characterization of Solid-Supported Lipid Bilayers Formed by Langmuir–Blodgett Deposition: A Tutorial. *Langmuir* **2018**, *34* (51), 15622–15639. https://doi.org/10.1021/acs.langmuir.8b03504.

(28) Lind, T. K.; Cárdenas, M. Understanding the Formation of Supported Lipid Bilayers via Vesicle Fusion-A Case That Exemplifies the Need for the Complementary Method Approach (Review). *Biointerphases* **2016**, *11* (2), 020801. https://doi.org/10.1116/1.4944830.

(29) Richter, R. P.; Bérat, R.; Brisson, A. R. Formation of Solid-Supported Lipid Bilayers: An Integrated View. *Langmuir* **2006**, *22* (8), 3497–3505. https://doi.org/10.1021/la052687c.

(30) Goodchild, J. A.; Walsh, D. L.; Connell, S. D. Nanoscale Substrate Roughness Hinders Domain Formation in Supported Lipid Bilayers. *Langmuir* **2019**, *35* (47), 15352–15363. https://doi.org/10.1021/acs.langmuir.9b01990.

(31) Scomparin, C.; Lecuyer, S.; Ferreira, M.; Charitat, T.; Tinland, B. Diffusion in Supported Lipid Bilayers: Influence of Substrate and Preparation Technique on the Internal Dynamics. *Eur. Phys. J. E* **2009**, *28* (2), 211–220. https://doi.org/10.1140/epje/i2008-10407-3.

(32) Schäfer, J.; Nehls, J.; Schön, M.; Mey, I.; Steinem, C. Leaflet-Dependent Distribution of PtdIns[4,5]P2 in Supported Model Membranes. *Langmuir* **2020**, *36* (5), 1320–1328. https://doi.org/10.1021/acs.langmuir.9b03793.

(33) Guo, L.; Har, J. Y.; Sankaran, J.; Hong, Y.; Kannan, B.; Wohland, T. Molecular Diffusion Measurement in Lipid Bilayers over Wide Concentration Ranges: A Comparative Study. *ChemPhysChem* **2008**, *9* (5), 721–728. https://doi.org/10.1002/cphc.200700611.

(34) Baumann, M. K.; Amstad, E.; Mashaghi, A.; Textor, M.; Reimhult, E. Characterization of Supported Lipid Bilayers Incorporating and Phosphoinositol-3,4,5-Triphosphate by Complementary Techniques. *Biointerphases* **2010**, *5* (4), 114–119. https://doi.org/10.1116/1.3516485.

(35) Braunger, J. A.; Kramer, C.; Morick, D.; Steinem, C. Solid Supported Membranes Doped with PIP2: Influence of Ionic Strength and pH on Bilayer Formation and Membrane Organization. *Langmuir ACS J. Surf. Colloids* **2013**, *29* (46), 14204–14213.

(36) Shi, X.; Kohram, M.; Zhuang, X.; Smith, A. W. Interactions and Translational Dynamics of Phosphatidylinositol Bisphosphate (PIP2) Lipids in Asymmetric Lipid Bilayers. *Langmuir* **2016**, *32* (7), 1732–1741. https://doi.org/10.1021/acs.langmuir.5b02814.

(37) Tero, R. Substrate Effects on the Formation Process, Structure and Physicochemical Properties of Supported Lipid Bilayers. *Materials* **2012**, *5* (12), 2658–2680. https://doi.org/10.3390/ma5122658.

(38) Visco, I.; Chiantia, S.; Schwille, P. Asymmetric Supported Lipid Bilayer Formation via Methyl-β-Cyclodextrin Mediated Lipid Exchange: Influence of Asymmetry on Lipid Dynamics and Phase Behavior. *Langmuir* **2014**, *30* (25), 7475–7484. https://doi.org/10.1021/la500468r.

(39) Vázquez, R. F.; Ovalle-García, E.; Antillón, A.; Ortega-Blake, I.; Bakás, L. S.; Muñoz-Garay, C.; Maté, S. M. Asymmetric Bilayers Mimicking Membrane *Rafts* Prepared by Lipid Exchange: Nanoscale Characterization Using AFM-Force Spectroscopy. *Biochim. Biophys. Acta BBA - Biomembr.* **2021**, *1863* (1), 183467. https://doi.org/10.1016/j.bbamem.2020.183467.

(40) Stanglmaier, S.; Hertrich, S.; Fritz, K.; Moulin, J.-F.; Haese-Seiller, M.; Rädler, J. O.; Nickel, B. *Asymmetric Distribution of Anionic Phospholipids in Supported Lipid Bilayers*. ACS Publications. https://doi.org/10.1021/la3019887.

(41) Enoki, T. A.; Feigenson, G. W. Asymmetric Bilayers by Hemifusion: Method and Leaflet Behaviors. *Biophys. J.* **2019**, *117* (6), 1037–1050. https://doi.org/10.1016/j.bpj.2019.07.054.

(42) Stanglmaier, S.; Hertrich, S.; Fritz, K.; Moulin, J. F.; Haese-Seiller, M.; Rädler, J. O.; Nickel, B. Asymmetric Distribution of Anionic Phospholipids in Supported Lipid Bilayers. *Langmuir* **2012**, *28* (29), 10818–10821. https://doi.org/10.1021/la3019887.

(43) Sun, Y.; Zang, X.; Sun, Y.; Wang, L.; Gao, Z. Lipid Membranes Supported by Planar Porous Substrates. *Chem. Phys. Lipids* **2020**, *228*, 104893. https://doi.org/10.1016/j.chemphyslip.2020.104893.

(44) Heo, P.; Ramakrishnan, S.; Coleman, J.; Rothman, J. E.; Fleury, J. B.; Pincet, F. Highly Reproducible Physiological Asymmetric Membrane with Freely Diffusing Embedded Proteins in a 3D-Printed Microfluidic Setup. *Small* **2019**, *15* (21), 1–13. https://doi.org/10.1002/smll.201900725.

(45) Liu, P.; Zabala-Ferrera, O.; Beltramo, P. J. Fabrication and Electromechanical Characterization of Freestanding Asymmetric Membranes. *Biophys. J.* **2021**, *120* (9), 1755–1764. https://doi.org/10.1016/j.bpj.2021.02.036.

(46) Campillo, C.; Sens, P.; Köster, D.; Pontani, L.-L.; Lévy, D.; Bassereau, P.; Nassoy, P.; Sykes, C. Unexpected Membrane Dynamics Unveiled by Membrane Nanotube Extrusion. *Biophys. J.* **2013**, *104* (6), 1248–1256.

(47) Ma, Y.; Benda, A.; Kwiatek, J.; Owen, D. M.; Gaus, K. Time-Resolved Laurdan Fluorescence Reveals Insights into Membrane Viscosity and Hydration Levels. *Biophys. J.* **2018**, *115* (8), 1498–1508. https://doi.org/10.1016/j.bpj.2018.08.041.

(48) Chazotte, B. Labeling Membranes with Carbocyanine Dyes (Dils) as Phospholipid Analogs. *Cold Spring Harb. Protoc.* **2011**, *6* (1), 76–80. https://doi.org/10.1101/pdb.prot5555.

(49) Moens, P. D. J.; Bagatolli, L. A. Profilin Binding to Sub-Micellar Concentrations of Phosphatidylinositol (4,5) Bisphosphate and Phosphatidylinositol (3,4,5) Trisphosphate. *Biochim. Biophys. Acta - Biomembr.* **2007**, *1768* (3), 439–449. https://doi.org/10.1016/j.bbamem.2006.12.012.

(50) Walsh, J. P.; Suen, R.; Glomset, J. A. Arachidonoyl-Diacylglycerol Kinase SPECIFIC IN VITRO INHIBITION BY POLYPHOSPHOINOSITIDES SUGGESTS A MECHANISM FOR REGULATION OF PHOSPHATIDYLINOSITOL BIOSYNTHESIS (*). *J. Biol. Chem.* **1995**, *270* (48), 28647–28653. https://doi.org/10.1074/jbc.270.48.28647.

(51) Richter, R. P.; Bérat, R.; Brisson, A. R. Formation of Solid-Supported Lipid Bilayers: An Integrated View. *Langmuir* **2006**, *22* (8), 3497–3505. https://doi.org/10.1021/la052687c.

(52) Beber, A.; Taveneau, C.; Nania, M.; Tsai, F.-C.; Di Cicco, A.; Bassereau, P.; Lévy, D.; Cabral, J. T.; Isambert, H.; Mangenot, S.; Aurélie, B. Membrane Reshaping by Micrometric Curvature Sensitive Septin Filaments. *Nat. Commun.* **2019**, *10* (1), 420.

(53) Gerelli, Y.; Porcar, L.; Lombardi, L.; Fragneto, G. Lipid Exchange and Flip-Flop in Solid Supported Bilayers. *Langmuir* **2013**, *29* (41), 12762–12769. https://doi.org/10.1021/la402708u.

(54) Beber, A.; Alqabandi, M.; Prévost, C.; Viars, F.; Lévy, D.; Bassereau, P.; Bertin, A.; Mangenot, S. Septin-Based Readout of PI(4,5)P2 Incorporation into Membranes of Giant Unilamellar Vesicles. *Cytoskeleton* **2019**, *76* (1), 92–103. https://doi.org/10.1002/cm.21480.

(55) Shukla, S.; Jin, R.; Robustelli, J.; Zimmerman, Z. E.; Baumgart, T. PIP2 Reshapes Membranes through Asymmetric Desorption. *Biophys. J.* **2019**, *117* (5), 962–974. https://doi.org/10.1016/j.bpj.2019.07.047.

(56) Meredith, S. A.; Kusunoki, Y.; Connell, S. D.; Morigaki, K.; Evans, S. D.; Adams, P. G. Self-Quenching Behavior of a Fluorescent Probe Incorporated within Lipid Membranes Explored Using Electrophoresis and Fluorescence Lifetime Imaging Microscopy. *J. Phys. Chem. B* **2023**, *127* (8), 1715–1727. https://doi.org/10.1021/acs.jpcb.2c07652.

(57) Wen, Y.; Vogt, V. M.; Feigenson, G. W. PI(4,5)P2 Clustering and Its Impact on Biological Functions. *Annu. Rev. Biochem.* **2021**.

(58) Ellenbroek, W. G.; Wang, Y. H.; Christian, D. A.; Discher, D. E.; Janmey, P. A.; Liu, A. J. Divalent Cation-Dependent Formation of Electrostatic PIP2 Clusters in Lipid Monolayers. *Biophys. J.* **2011**, *101* (9), 2178–2184. https://doi.org/10.1016/j.bpj.2011.09.039.

(59) McIntosh, B. B.; Ostap, E. M. Myosin-I Molecular Motors at a Glance. *J. Cell Sci.* **2016**, *129* (14), 2689–2695.

(60) Pyrpassopoulos, S.; Feeser, E. A.; Mazerik, J. N.; Tyska, M. J.; Ostap, E. M. Membrane-Bound Myo1c Powers Asymmetric Motility of Actin Filaments. *Curr. Biol.* **2012**, *22* (18), 1688–1692.

(61) Pernier, J.; Kusters, R.; Bousquet, H.; Lagny, T.; Morchain, A.; Joanny, J. F.; Bassereau, P.; Coudrier, E. Myosin 1b Is an Actin Depolymerase. *Nat. Commun.* **2019**, *10* (1), 1–7. https://doi.org/10.1038/s41467-019-13160-y.

(62) Fellmann, P.; Hervé, P.; Pomorski, T.; Müller, P.; Geldwerth, D.; Herrmann, A.; Devaux, P. F. Transmembrane Movement of Diether Phospholipids in Human Erythrocytes and Human Fibroblasts. *Biochemistry* **2000**, *39* (17), 4994–5003. https://doi.org/10.1021/bi992649q.

(63) Rodriguez, N.; Amarouch, M. Y.; Montnach, J.; Piron, J.; Labro, A. J.; Charpentier, F.; Mérot, J.; Baró, I.; Loussouarn, G. Phosphatidylinositol-4,5-Bisphosphate (PIP2) Stabilizes the Open Pore Conformation of the Kv11.1 (hERG) Channel. *Biophys. J.* **2010**, *99* (4), 1110–1118. https://doi.org/10.1016/j.bpj.2010.06.013.

(64) Pincet, F.; Adrien, V.; Yang, R.; Delacotte, J.; Rothman, J. E.; Urbach, W.; Tareste, D. FRAP to Characterize Molecular Diffusion and Interaction in Various Membrane Environments. *PLoS ONE* **2016**, *11* (7), 1–19. https://doi.org/10.1371/journal.pone.0158457.

(65) Yamada, A.; Mamane, A.; Lee-Tin-Wah, J.; Di Cicco, A.; Prévost, C.; Lévy, D.; Joanny, J. F.; Coudrier, E.; Bassereau, P. Catch-Bond Behaviour Facilitates Membrane Tubulation by Non-Processive Myosin 1b. *Nat. Commun.* **2014**, *5*, 3624. https://doi.org/10.1038/ncomms4624.

(66) Spudich, J. A.; Watt, S. The Regulation of Rabbit Skeletal Muscle Contraction. *J. Biol. Chem.* **1971**, *246* (15), 4866–4871. https://doi.org/10.1016/s0021-9258(18)62016-2.

Supplementary information

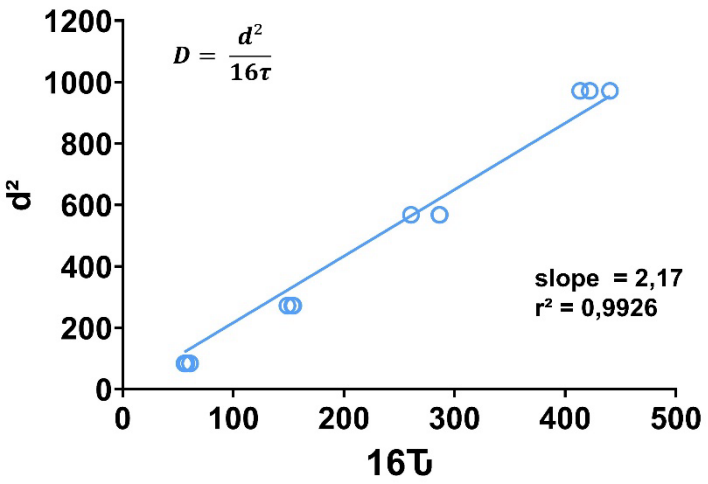

Supplementary Figure 1. *Example of data fitting to determine the diffusion coefficient of lipids for one set of FRAP measurements. Each point represents a single FRAP experiment at a given area diameter d (μm) and characteristic time τ (sec) of a FRAP recovery.*

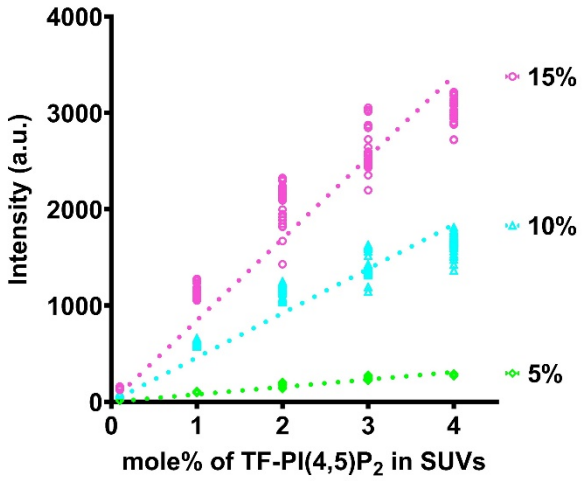

Supplementary Figure 2. *TF-PI(4,5)P_2 fluorescent intensities in sym-SLBs generated by using SUVs containing concentrations of TF-PI(4,5)P_2 ranging from 0.1 mole% to 4 mole%. The TF-PI(4,5)P_2-sym-SLBs were imaged using three different laser powers, 5, 10 and 15% by a 488 nm laser with a maximum laser power of 100 mW in a spin-disk confocal microscope.*